Research Article

Li Xie, Xiao Hu*, Zhong Xu*, ZhenLin Chen, PengBo Wang, and RuiZheng Liang

Experimental study on comprehensive improvement of shear strength and erosion resistance of yellow mud in Qiang Village

https://doi.org/10.1515/rams-2022-0040
received March 27, 2022; accepted April 22, 2022

Abstract: To achieve better mechanical properties and higher scour resistance of yellow mud in Qiang Village, this study investigated how to improve yellow mud by single factors of straw, starch, cement, and epoxy resin. First, the effect of each material on the shear strength of yellow mud was analyzed through the direct shear test, and the effect of the respective material on the scour resistance of yellow mud was examined using a self-made spray device. Subsequently, combined with the results of the two experiments, the improvement effect of the material was comprehensively studied, and the optimal dosage of the respective material was determined. Lastly, an electron microscope was used to observe the microscopic morphology of the samples, and the improvement mechanism of each material was discussed from qualitative and quantitative perspectives. As revealed by the results, straw, starch, cement, and epoxy resin improved the shear strength and scour resistance of yellow mud. Peaks of straw, starch, and epoxy resin were found in their corresponding properties-dosage curves, corresponding to the optimal dosage in the experimental range. The corresponding performance curve of cement showed a unidirectional change, which was found with a significant improvement effect.

Keywords: yellow mud in Qiang Village, modified material, shear strength, anti-scouring, microstructure

* **Corresponding author: Xiao Hu,** State Key Laboratory of Geohazard Prevention and Geoenvironment Protection, Chengdu University of Technology, Chengdu 610059, China, e-mail: huxiao@cdut.cn
* **Corresponding author: Zhong Xu,** State Key Laboratory of Geohazard Prevention and Geoenvironment Protection, Chengdu University of Technology, Chengdu 610059, China, e-mail: xuzhong@cdut.edu.cn
Li Xie, ZhenLin Chen, PengBo Wang, RuiZheng Liang: State Key Laboratory of Geohazard Prevention and Geoenvironment Protection, Chengdu University of Technology, Chengdu 610059, China

1 Introduction

The modern Qiang people primarily live in Maoxian, Wenchuan, Lixian, and Songpan in Aba Tibetan and Qiang Autonomous Prefecture in Sichuan Province, Beichuan Qiang Autonomous County and Pingwu County in Mianyang, as well as Danba County in Ganzi Tibetan Autonomous Prefecture (Figure 1) [1]. After the Wenchuan earthquake, a belt-shaped strong earthquake area was formed with a length of nearly 300 km following the line of Wenchuan-Maoxian-Beichuan-Pingwu-Qingchuan. During the earthquake, most Qiang buildings were partially damaged, with only one newly built building collapsing in Taoping Qiang Village, Li County. In general, Qiang village is structured as stone masonry, and the walls are made of local yellow mud as the bonding material. Compared with concrete mortar, yellow mud has low bonding ability [2]. Over time, yellow mud will fall off seriously, thus leading to a decrease in the wall strength. The wall will be easily damaged by earthquakes and rain [3,4]. Under natural disasters (e.g., earthquakes, rain erosion, and wind disasters), the walls of Qiang village are primarily manifested as wall cracks, wall surface soil shedding, and wall collapse (Figure 2). The architectural style of Qiang Village has been considered an integral part of national culture. From the perspectives of material selection and building site selection, the architectures of Qiang Village retain the characteristics of the original traditional dwellings, while retaining symbolic meaning and some long-standing architectural components and symbolic elements. Once these architectures are replaced with modern building materials and styles, folk culture will be significantly affected and destructed. Impacted by old and new architectural culture and the emergence of novel technologies, new materials, and new processes, the modification of raw soil materials has aroused increasing attention of scholars [5].

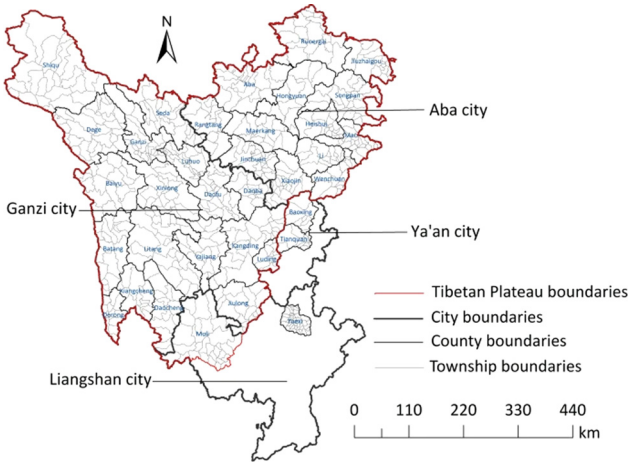

Figure 1: The distribution map of ethnic minorities in Sichuan [6].

Yellow mud of Qiang village is a type of raw soil. Raw soil architecture has been investigated in depth in numerous countries, and valuable results have been achieved [7,8]. With the emergence of novel materials and technologies, the modification technology of raw soil materials has been investigated widely [9,10]. The modified materials can be divided into physically modified materials and chemically modified materials in accordance with their modification mechanisms, compositions, and structures [11,12].

In general, physically modified materials consist of biological starch, glutinous rice, sucrose, plant rhizomes, water-reducing agents, etc. [13–15]. Xu used steel fiber and polyester fiber as the modified materials and found that the fiber was closely combined with the matrix. In addition, it was found that the modified materials could effectively transfer the force and enhance the properties of the matrix material [16,17]. Liu reinforced the soil using cotton straw fibers. The research result suggested that the unconfined compressive strength of fiber-reinforced soil decreased exponentially with the increase in the number of freeze-thaw cycles [18]. Li performed triaxial tests to investigate the effect of polypropylene fiber content and length on the mechanical properties exhibited by clay. The result suggested that when the polypropylene fiber length was controlled at 2.5 cm, and the fiber content was 0.3%, the sample could achieve the maximum strength, and the reinforcement effect was found the best [19]. Sujatha used alkali-resistant glass fiber and electronic-grade glass fiber as the reinforcement materials. The study suggested that both the glass fibers could increase the unconfined compressive strength and energy absorption capacity of the reinforced soil, and the optimal dosage was 0.75% [20]. Tang reinforced the soil with natural palm fibers, and performed micro-scale tests on the reinforced soil samples using polarized light and scanning electron microscopy (SEM) before and after the creep test. As revealed by the results, the fiber-reinforced material could inhibit the deformation of the soil and increase the long-term strength of the soil [21].

In general, chemically modified materials consist of slaked lime, desulfurized gypsum, cement, fly ash, slag, water glass, etc., [22–26]. Tiago Miranda incorporated activated alkaline fly ash into the mortar of masonry specimens. As revealed by the research result, the compressive and shear properties of the specimens were significantly enhanced [27]. Xu used a novel material mixed with cement, foam, polypropylene fibers, and water to reinforce soft soil foundations. It was found through triaxial shear tests that the triaxial shear strength and cohesion first increased and then decreased, and reached the peak when the reinforcement ratio was 0.75% [28]. Yue used industrial by-product phosphogypsum as the raw material, mixed it with slag and calcium-rich silicon active material to prepare a phosphogypsum-based roadbed stabilizer, and then modified it using active powder. The modified material was found as an effective roadbed stabilizer [29]. Portelinha treated diesel-contaminated red loam

Figure 2: Disease status of Qiang village wall (taken by author): (a) wall cracks; (b) wall surface soil falling off; and (c) wall collapse.

with lime and reported that the soil properties of diesel-contaminated soil could be significantly enhanced at the lime stabilizer dosage of 6% [30]. Nath reviewed the potential use of silico-manganese slag as a binder and aggregate in Portland cement and geopolymer concrete. He concluded that the slag was primarily used as an auxiliary cementitious material to enhance soil properties [31].

In brief, physically and chemically modified materials play a certain role in strengthening the raw soil. In this study, the above materials were used to modify yellow mud in Qiang Village. The Qiang Village has been well-preserved after having been through many earthquakes, which has aroused wide attention and interest of the scholars. Currently, the existing research on Qiang Village has mostly focused on its history and culture, architectural aesthetics, earthquake damage investigation, and tourism development, whereas there has been rare research on the material properties of the Qiang Village. Since the materials in Qiang Village has low strength, the walls are prone to cracks due to earthquakes. Accordingly, the strength of Qiang Village materials should be increased. Qiang Village is close to the mountains, and the local rainfall is year-round. During the modification of its yellow mud, the enhancement of erosion resistance should be highlighted besides the increase in strength.

Thus, it is necessary to find a material suitable for comprehensively increasing the strength and scour resistance of yellow mud in Qiang Village. In China, straw has a large output in rural areas, and most of the existing treatment methods have not met the requirements of environmental protection [32]. To achieve recycling, one of the modified materials in this study was straw. Starch, a naturally renewable resource characterized by a low price, adhesive film-forming, and degradability, has been applied in numerous fields [33]. Accordingly, starch was selected as the modified material in this study. Epoxy resin exhibits good chemical properties and corrosion resistance, and it has been largely used for the restoration of some ancient buildings, whereas it is rarely used for the modification of raw soil materials. Thus, epoxy resin was selected as a type of modified material in this study [34]. It was found through the investigation of Taoping Qiang Village that the stockade built over the past few years has completely replaced the yellow mud with cement, which has destroyed the style of the Qiang Village. This study aimed to explore a suitable amount of cement to allow the cement to enhance the performance of yellow mud without destroying its original style, and cement was also selected as the material.

As a result, straw, starch, cement, and epoxy resin were used in this study to modify the yellow mud. Through the direct shear test and the anti-scour test, the effect of the type and content of modified materials on the properties of yellow mud was investigated, and the optimal content of each material was measured. On that basis, the modification mechanisms of different materials were analyzed under the SEM. With the development of computer image processing technology, the quantification of soil microstructure has become possible, and a series of valuable achievements have been made [35–37]. In this study, the Pores and Cracks Analysis System (PCAS) was used to process the pictures scanned under the electron microscope, and the pictures were quantitatively analyzed based on the geometric parameters output by the software [38]. This study is expected to provide a reference for future research on earthquake resistance and disaster reduction in Qiang Village.

2 Materials and methods

Straw, starch, epoxy resin, and cement were used as the modified materials. The yellow mud of Qiang Village was modified through single mixing. Through the shear strength test, anti-scour test, and microscopic analysis of the modified raw soil sample, the changes in the modified raw soil sample during the test were observed and analyzed, and the test data were recorded. The ultimate bearing capacity and failure mechanism of the modified soil specimens were analyzed in depth, and the effect of the amount of modified materials on the mechanical properties of the samples was explored. Thus, this study can provide a reference for selecting a reasonable ratio of modified materials. Figure 3 illustrates the technical route.

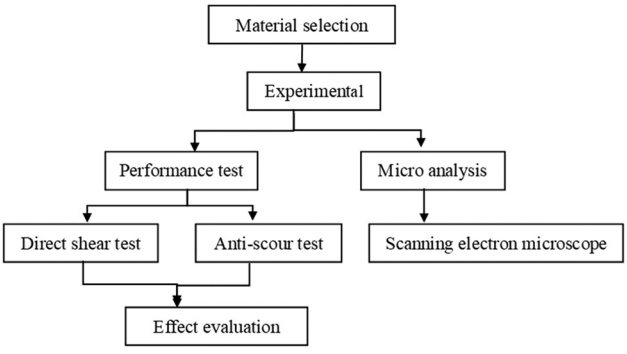

Figure 3: Technical route.

Figure 4: Yellow mud of Qiang Village.

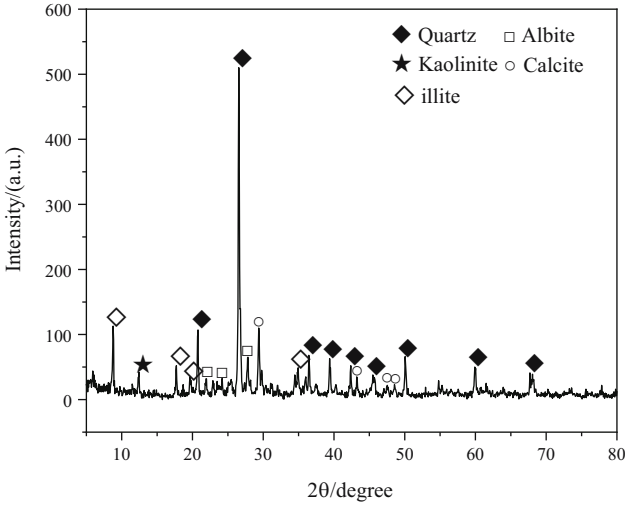

Figure 5: XRD of yellow mud.

2.1 Materials

The raw material for the test was yellow mud, which was taken from the mountains near Taoping Qiang Village, Li County, Aba Prefecture. Before the test specimens were prepared, the raw soil material should be left in the air for 1–2 days to evaporate the water in the soil. The raw soil particles were passed through the standard 5 mm coarse sieve, and thus, the soil particle size of the raw soil material used for the test could be ensured to be within 5 mm (Figure 4). Before the formal experiment, the basic indicators of yellow mud were obtained using drying method, compaction test, combined determination method of liquid-plastic limit, and X-ray diffraction. The soil was silty clay, which was largely composed of quartz, albite, kaolinite, calcite, and illite. Tables 1 and 2 and Figure 5 present other basic physical indicators.

In this study, straw, starch, cement, and epoxy resin were selected as the modified materials (Figure 6). The straw was bought online, and the length was controlled between 3 and 4 cm, and the surface of the straw was not smooth and had a large frictional force. The starch was from sweet potato, which was white in color and characterized by excellent adhesion and film-forming properties and degradability. Ordinary Portland cement was used as the cement in this study, and its main chemical components included SiO_2, Al_2O_3, CaO, Fe_2O_3, MgO, SO_3, P_2O_5, Na_2O, etc. The model E-51 epoxy resin and T-31 curing agent were used in the ratio of 4:1. It was characterized by stable chemical properties, strong adhesion, and low shrinkage.

2.2 Testing programme

2.2.1 Preparation of samples

The specimens were assigned into 17 groups, including plain soil control group (group A), 0.25% straw (group B1), 0.5% straw (group B2), 0.75% straw (group B3), 1% straw (group B4), 1% starch (group C1), 3% starch (group C2), 5% starch (group C3), 7% starch (group C4), 2% cement (group D1), 5% cement (group D2), 8% cement

Table 1: Particle size distribution

	<0.075 mm	0.075–0.25 mm	0.25–0.5 mm	0.5–1 mm	1–2 mm	>2 mm
Particle distribution (%)	72.56	2.64	2.85	4.67	6.30	10.98

Table 2: Basic physical property indexes of yellow mud

Natural moisture content (%)	Optimal moisture content (%)	Maximum dry density (g·cm^{-3})	Liquid limit (%)	Plastic limit (%)	Plasticity index
1.82	19.47	1.68	29.27	18.67	10.6

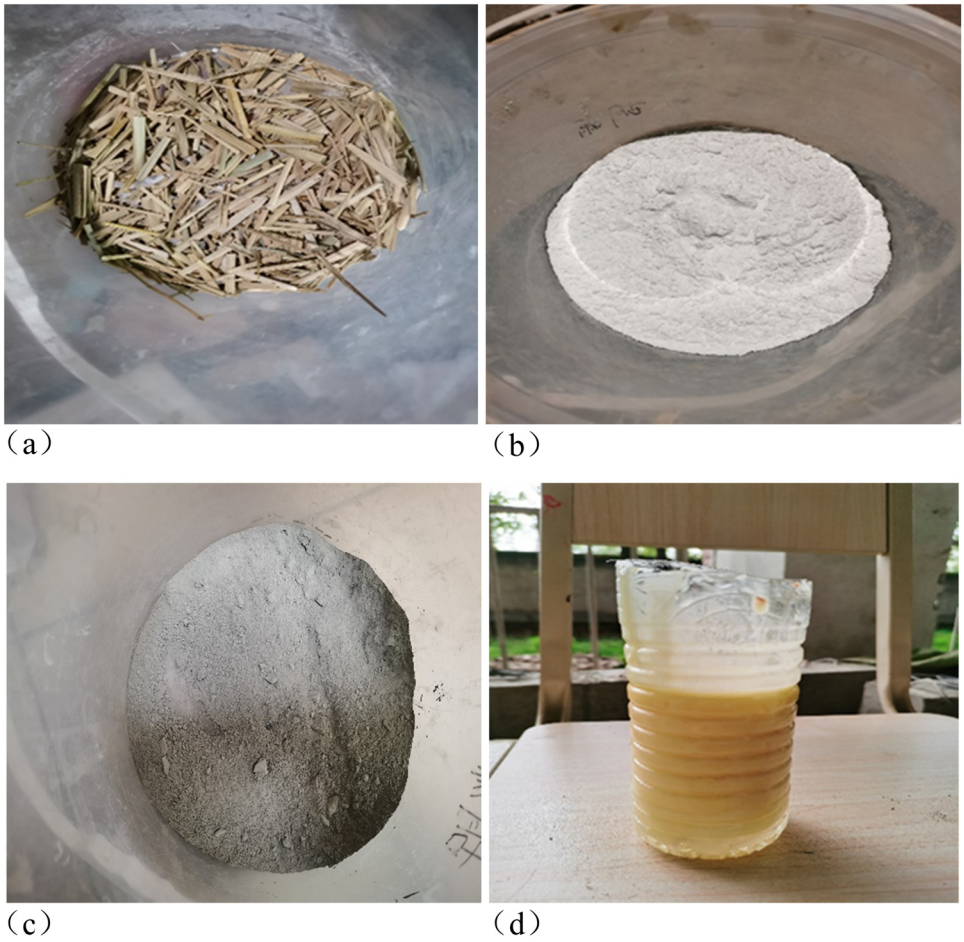

Figure 6: Modified material: (a) straw; (b) starch; (c) cement; and (d) epoxy resin.

(group D3), 11% cement (group D4), 3% epoxy resin (group E1), 5% epoxy resin (group E2), 7% epoxy resin (group E3), as well as 11% epoxy resin (group E4). In accordance with the "Standards for Geotechnical Test Methods" (GB/T50123-2019), the round cake-shaped raw soil specimens with a diameter of 61.8 mm and a height of 20 mm were employed for direct shearing test, and there were a total number of 68 specimens. A mold with a size of 100 mm × 100 mm × 100 mm was used to make cube-shaped raw soil specimens for the anti-scour test, and the total number of specimens was 51. After the specimens were prepared, they were cured in a natural state (Figure 7). Table 3 lists the material ratio of the specimen, and Table 4 depicts the main equipment and instruments of the test.

2.2.2 Direct shear test

The direct shear test was performed using a quadruple constant strain direct shear tester (Figure 8). In this test, a sample with a diameter of 61.8 mm and a height of 20 mm was applied, and the shear rate was set at 0.8 mm·min^{-1}. Under no lateral deformation, the vertical pressures including 100, 200, 300, and 400 kPa were applied to the 4 raw soil specimens, respectively. Before the test was performed, the balance weight of the direct shearing instrument should be adjusted to level the pressure lever, and Vaseline was applied evenly on the inner wall of the shearing box to reduce the effect of resistance. Before the test piece was installed, the upper and lower boxes of the shearing container should be aligned before the fixing pin was inserted. The permeable plate and filter paper were placed in the box. Subsequently, the test piece was gently placed in the box, and the filter paper and the permeable plate were placed on the test piece. Lastly, the pin was removed, and the cutting began. During the shearing process, the test block underwent shear failure along the horizontal direction of the shear box, thus resulting in displacement (Figure 9). Accordingly, the shear stress τ of the specimen on the shear plane when shear failure occurred, and the shear strength parameters, cohesion c and internal friction angle φ, were calculated according to Coulomb's law.

Figure 7: Forming sample.

2.2.3 Anti-scour test

In this test, 100 mm × 100 mm × 100 mm cube-shaped raw soil specimens were used. To be specific, a total of 17 groups were involved, of which each was tested with 3 specimens. The average value was taken as the final value. During the test, a sprinkler head, a rubber hose, a pressure gauge, tap water, and others were used as a set of sprinkler devices (Figure 10). Based on the rainfall in Lixian County over the past few years, the parameters applied in this test to simulate rainfall included: the distance from the nozzle to the specimen was 30 cm, the diameter of the nozzle was 8 cm, there were 52 nozzle holes with a diameter of 1 mm, and the water pressure ranged from 0.05 to 0.07 MPa. The test pieces were put on the iron net one by one, and the nozzles were fixed to ensure that the water flow was sprayed down to the test pieces, the flow of the water was adjusted, and the water pressure was controlled. Natural precipitation was simulated to perform a spray test on the surface of the raw soil specimen, the spraying time and surface changes were observed, and the size of the specimen was measured every 10 min. Lastly, the volume loss rate of the specimen was calculated after 60 min, and the average value of the respective group was taken. On that basis, the anti-scour performance of the test piece in the spray test was examined.

Table 3: Ratio of materials

Numbering	Material	Dosage
A	Yellow mud	100%
B	Straw	0.25, 0.5, 0.75, and 1%
C	Starch	1, 3, 5, and 7%
D	Cement	2, 5, 8, and 11%
E	Epoxy resin	3, 5, 7, and 10%

Table 4: Main test instruments and equipment

Equipment	Model
Classifier	5 mm
Electronic scale	YP3002N
Specimen mold box	100 mm × 100 mm × 100 mm
Concrete vibration table	ZD/LX–PTP
Quadruple equal strain direct shear apparatus	DJY-4L
SEM	S-3000N

Figure 8: Quadruple constant strain direct shear apparatus.

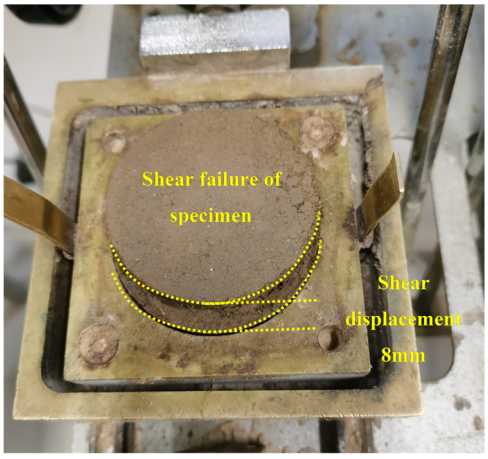

Figure 9: Shear failure of test block.

2.2.4 Microstructure

After the direct shear test and the anti-scour test were performed, the improvement effect of different contents of the respective material was analyzed, and the sample mixed with straw, starch, cement, and epoxy resin was selected as the test sample. It was cut into soil sample of 8 mm × 8 mm × 15 mm. Subsequently, it was sprayed with metal coating and observed by SEM (Thermo Fisher Scientific's Prisma-E) (Figure 11).

Figure 10: Self-made sprinkler.

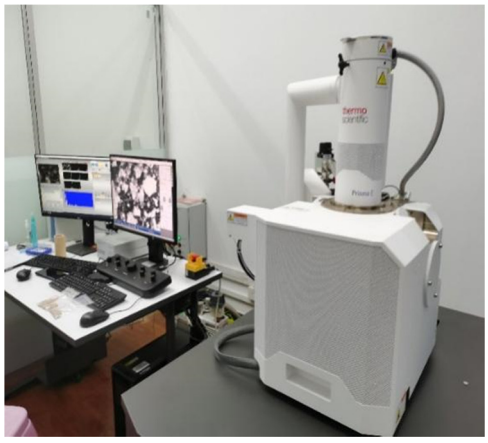

Figure 11: Electron microscope scanner.

3 Experimental results and discussion

The shear strength, scour loss rate, and apparent characteristics were determined through the direct shear and scour tests of 34 groups of improved loess and the SEM analysis. The strength improvement effect was expressed using the ratio of shear strength of modified yellow mud to pure yellow mud, and the anti-scour ability of specimens was characterized using the scour coefficient. The improvement effect of different modified materials and dosage on Taoping Qiang Village yellow mud was analyzed in depth.

3.1 Analysis of direct shear test results

3.1.1 Analysis of shear strength index

Figure 12 presents the change in shear strength of specimens with different material dosages, and Figure 13 illustrates the shear strength index of specimens with different material dosages.

Figure 12a shows the strength change in the straw-modified yellow mud specimen. As depicted in Figure 12a, when the straw content was 0.5%, the shear strength of the specimen reached its peak value. Under different vertical pressures, the corresponding shear strengths were 76.8, 123.69, 176.6, and 225.4 kPa, 12.64–20% higher than those of the pure yellow mud specimens. As depicted in Figure 13a, the shear strength index of the specimen changed with the increase in the straw content. When the straw content was 0.5%, both the cohesion and internal friction angle of the specimen reached their peaks, including

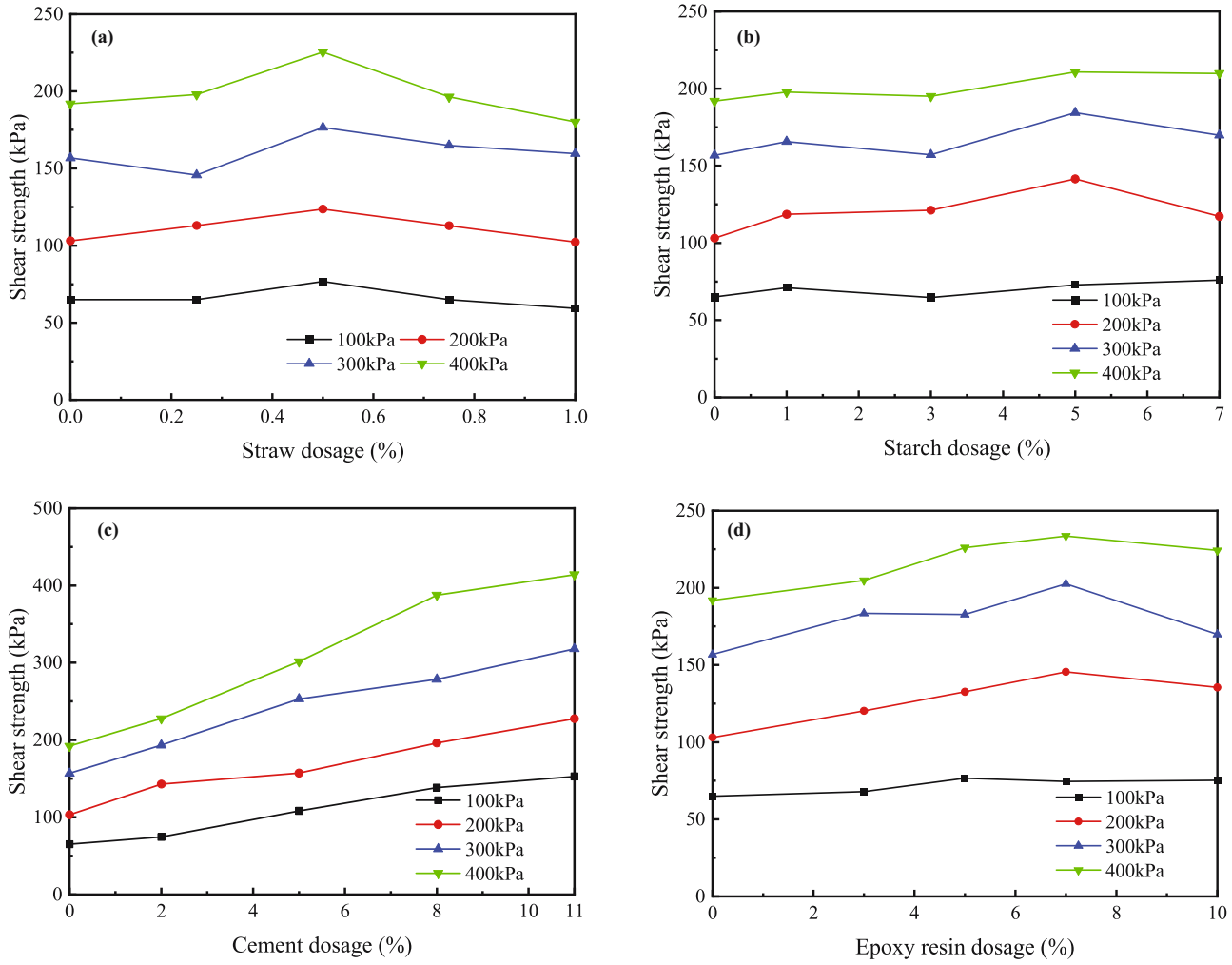

Figure 12: Change in shear strength of yellow mud with different material contents: (a) straw; (b) starch; (c) cement; and (d) epoxy resin.

25.95 kPa and 26.51°, respectively, 26.13 and 13.9% higher than those of the pure yellow mud specimen. This was due to the tie effect of the straw, which increased the cohesion of the specimen; the surface of the straw had irregular grooves, thus increasing the occlusal force between the soil and the material and increasing the internal friction angle of the soil. When the straw content was higher than 0.5%, the shear strength index of the specimens decreased. This was because the straw was hollow inside (SEM figure). When the doping amount was too high, the pores inside the straw were connected in the specimen, thus increasing the weak points inside the specimen and ultimately resulting in reduction in the shear strength, cohesion, and internal friction angle of the specimen. Thus, straw dosage is recommended to be controlled at 0.5%

Figure 12b shows strength changes of starch-modified yellow mud. As depicted in Figure 12b, when the starch content was 5%, the shear strength of the specimen reached the peak. Under different vertical pressures, the corresponding shear strength was 72.9, 141.5, 184.4, and 210.8 kPa, respectively, 9.83–37.28% higher than that of the pure yellow mud specimens. As depicted in Figure 13b, the shear strength index of the specimen increased first and then decreased with the increase in the straw content. When the straw content was 5%, the cohesion and internal friction angle of the specimen reached the peaks of 38.2 kPa and 24.5°, respectively, 85.71 and 5.29% higher than those of the pure yellow mud specimen. This was because the gelation of starch made the soil better bond together, thus improving the cohesion and internal friction angle of the specimen. When the dosage was too high, the shear strength index of the specimens decreased. This was because when the starch content was too much, the starch tended to cluster (SEM figure). The above starch groups increased the weak area inside the specimen, and the soil could not be wrapped with enough starch, thus resulting in reduction in the shear strength,

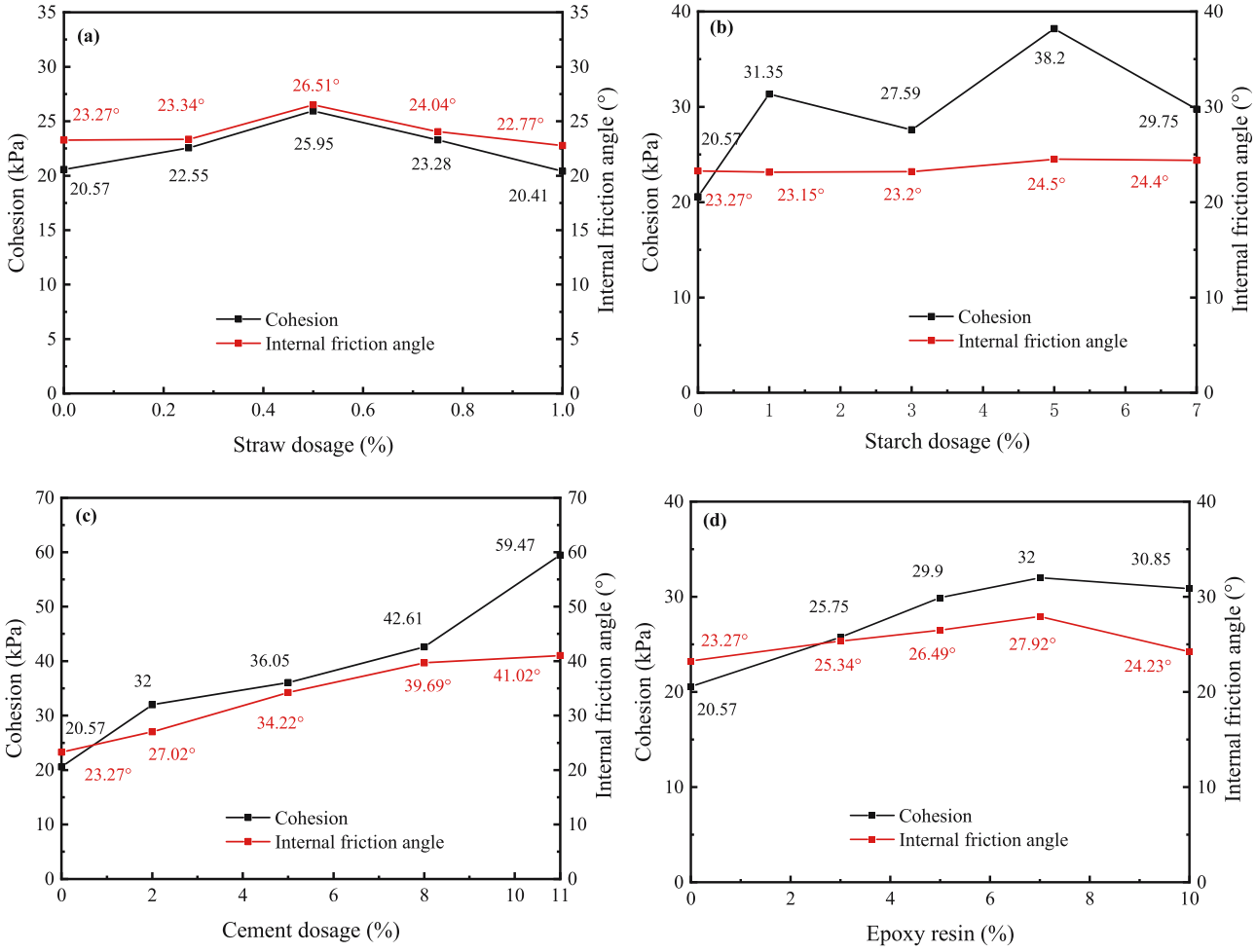

Figure 13: Shear strength indexes of different materials: (a) straw; (b) starch; (c) cement; and (d) epoxy resin.

cohesion, and internal friction angle of the specimens. Accordingly, the starch content is recommended to be controlled at 5%.

Figure 12c illustrates the strength changes in cement improved yellow mud. As depicted in Figure 12c, the shear strength of specimens increased with the increase in the cement content. When the vertical pressure was 400 kPa, the shear strength corresponding to different cement contents was 227.64, 301.4, 387.46, and 414.074 kPa, respectively, which increased by 18.58–115.74% compared with pure yellow mud specimens. As depicted in Figure 13c, the higher the cement content, the higher the shear strength index of the specimen would be. The cohesive force corresponding to different cement contents was 32, 36.05, 42.61, and 59.47 kPa, marking the increases by 55.57–189.11% compared with yellow mud samples. The internal friction angles corresponding to different cement contents were 27.02°, 34.22°, 39.69°, and 41.02°, 16.12–76.28% higher than those of yellow mud specimens. The reason was that after the yellow mud was mixed with cement, the fine cement particles and hydration products played a significant filling effect and decreased the number of pores. Moreover, the hydration of cement produced hydraulic gel products, which increased the cohesion between loose yellow mud particles, thus improving the shear strength of the samples. As revealed by the situation of Taoping Qiang Village in Li County, the newly built village over the past few years has completely replaced the yellow mud with cement, which has destroyed the style of the Qiang Village. Some scholars have shown that when the cement content is 11%, the raw soil material is stable enough [22,23]. Furthermore, according to "Code for Design of Masonry Structure" GB50003-2011, the shear strength standard of stone masonry mortar is 170 kPa. According to the local construction experience multiplied by the safety factor of 1.77, 300.9 kPa already satisfies the local strength requirements. When the cement content is 5%, the shear strength is 301.4 kPa, which has

exceeded the standard requirement. Combined with the current market price of cement, the cost of different cement dosages has been rising (Figure 14). Based on the above two indicators, for the shear resistance of the specimen, the cement content is recommended to be controlled at 5%.

Figure 12d illustrates the strength change in epoxy resin-modified yellow clay. As depicted in this figure, the shear strength first increased and then decreased with the increase in epoxy resin content; it reached a peak when the content of epoxy resin was 7%. Under different vertical pressures, the corresponding shear strengths were 74.5, 155.6, 202.6, and 233.6 kPa, marking the increases by 14.61–41.26%. As depicted in Figure 13d, the cohesion and internal friction angle of the specimens were consistent, and peaks were reached when the dosage was 7%, which were 32 kPa and 27.92°, respectively, marking the increases by 55.57 and 19.98%, respectively. Since the three-dimensional (3D) network structure formed by epoxy resin in the modification process wrapped the soil in it, the internal connection of the soil was more tight, and the network structure would increase the surface friction and occlusal force between the particles. Thus, with the increase in epoxy resin content, the cohesion and internal friction angle of the soil would be larger. When the dosage was 7%, the pores inside the specimen were rare, and the soil was well wrapped. Accordingly, when the dosage increased again, the shear strength indexes did not change much. Thus, the dosage of epoxy resin is recommended to be controlled at 7%.

3.1.2 Shear stress–shear displacement curve analysis

To analyze the deformation characteristics of the samples at different stages, the shear stress–shear displacement curves of 0.5% straw, 5% starch, 11% cement, and 7% epoxy resin were plotted for the specimens characterized by the maximum shear strength. The deformation of the sample could fall into three main stages, including elastic deformation, plastic deformation, and shear failure, in accordance with the change rule of the above curves. At the elastic deformation stage, the shear stress increased rapidly and linearly with the shear displacement. At this stage, the specimen was primarily in the elastic deformation, and the corresponding shear stress at the end of the curve was proportional strength τ_e. At the plastic deformation stage, the shear stress increased slowly, and the corresponding shear stress at the end of the curve was the shear strength τ_f. At the shear failure stage, the shear stress will reach a peak point, after which, as the shear strain continues to grow, the shear stress will form a descending section until the specimen is completely destroyed. Finally, there was a relatively stable residual shear strength τ_p. In this study, the end of the curve of shear stress and shear displacement with approximate linear growth was considered the end of the first stage, and the point corresponding to the shear strength displayed on the device of geotechnical test data acquisition system was recognized as the end of the second stage. Table 5 lists the shear displacements corresponding to the ends of the elastic and plastic stages.

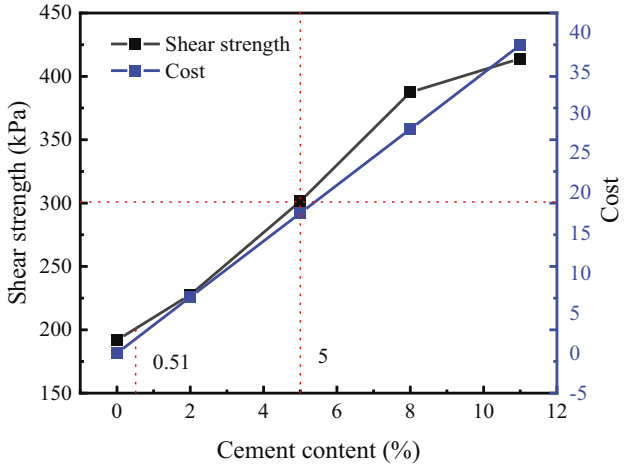

Figure 14: Influence of strength and cost on cement content.

Figure 15 presents the shear stress–shear displacement curve of pure yellow mud, belonging to the strain hardening type. Figure 15 and Table 5 depict that the elastic deformation stage of the pure yellow mud specimen under different vertical pressures ends when the shear displacement reached 1.17, 1.06, 1.66, and 2.19 mm, and the plastic deformation stage ended at 3.9, 4.01, 4, and 3.93 mm. By averaging the elastic deformation and plastic deformation under different vertical pressures, it was found that the corresponding elastic deformation and plastic deformation of the pure yellow mud specimen were 1.52 and 2.44 mm.

Figure 16 illustrates the strength characteristic curve of yellow mud treated with different materials. As depicted in this figure, the curves of adding 0.5% straw, 5% starch, and 7% epoxy resin were the same as those of pure yellow mud. Figure 16c presents the strength characteristic curve of the specimen after the cement treatment, belonging to the strain softening type, thus revealing that the shear failure was brittle and had a significant peak value. After exceeding the peak value, the shear stress tended to decrease with the increase in the shear displacement, high residual strength was maintained, and the strength enhancement effect was obvious.

Table 5 lists the corresponding shear displacement at the end of the respective stage. The table indicates that

Table 5: Shear displacement at the end of the respective stage

	First stage of final shear displacement (mm)				Second stage of final shear displacement (mm)				Average elastic deformation (mm)	Average plastic deformation (mm)
	100 kPa	200 kPa	300 kPa	400 kPa	100 kPa	200 kPa	300 kPa	400 kPa		
Yellow mud	1.17	1.06	1.66	2.19	3.90	4.01	4.00	3.93	1.52	2.73
0.5% straw	0.51	0.65	0.72	0.78	3.94	4.08	3.81	3.94	0.67	3.43
5% starch	1.44	1.30	1.61	2.15	3.83	3.95	3.93	3.96	1.63	2.39
11% cement	0.41	1.02	0.87	1.41	2.19	2.00	2.07	2.01	0.93	1.94
7% epoxy resin	1.07	1.26	1.62	2.25	3.96	4.28	4.24	4.00	1.55	2.89

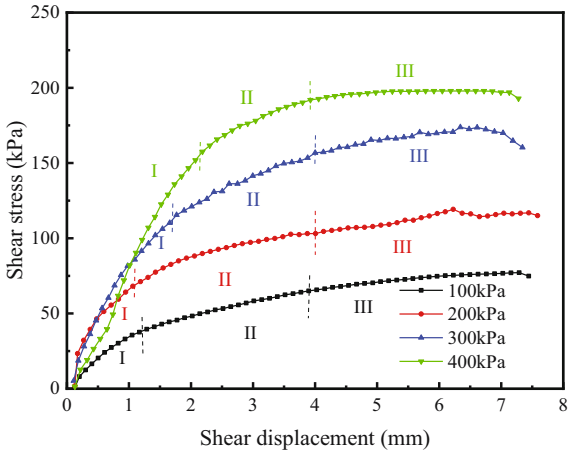

Figure 15: Shear stress–shear displacement curve of yellow mud.

the average elastic deformation of the test piece with 0.5% straw under different vertical pressures was obtained as 0.67 mm, 55.92% less than that of the pure yellow mud test piece, and the average plastic deformation was measured as 3.28 mm, 34.43% more than that of the pure yellow mud test piece. The average elastic deformation of the specimen with 5% starch under different vertical pressures was obtained as 1.63 mm, 7.24% higher than that of the pure yellow mud specimen, and the average plastic deformation was 2.39 mm, 12.45% lower than that of the pure yellow mud specimen. The average elastic deformation of the specimen with 11% cement under different vertical pressures measured 0.93 mm, 38.82% less than that of the pure yellow mud specimen, and the average plastic deformation was found as 1.94 mm, 28.93% less than that of the pure yellow mud specimen. The average elastic deformation of the specimen with 7% epoxy resin under different vertical pressures was found as 1.55 mm, 1.97% higher than that of the pure yellow clay specimen, and the average plastic deformation was obtained as 2.89 mm, 5.86% higher than that of the pure yellow clay specimen.

3.2 Analysis of anti-scouring test results

17 groups of specimens were scoured, 3 specimens were tested in each group, and the average value was taken as the final value. Figure 17 presents the apparent characteristics of the respective material specimen after scouring. After the test piece mixed with straw was washed, the surface was damaged and had holes, and the straw was exposed. After the test piece mixed with starch was washed, holes were generated on the upper surface, and there were cracks on the edge and the surrounding soil was falling off.

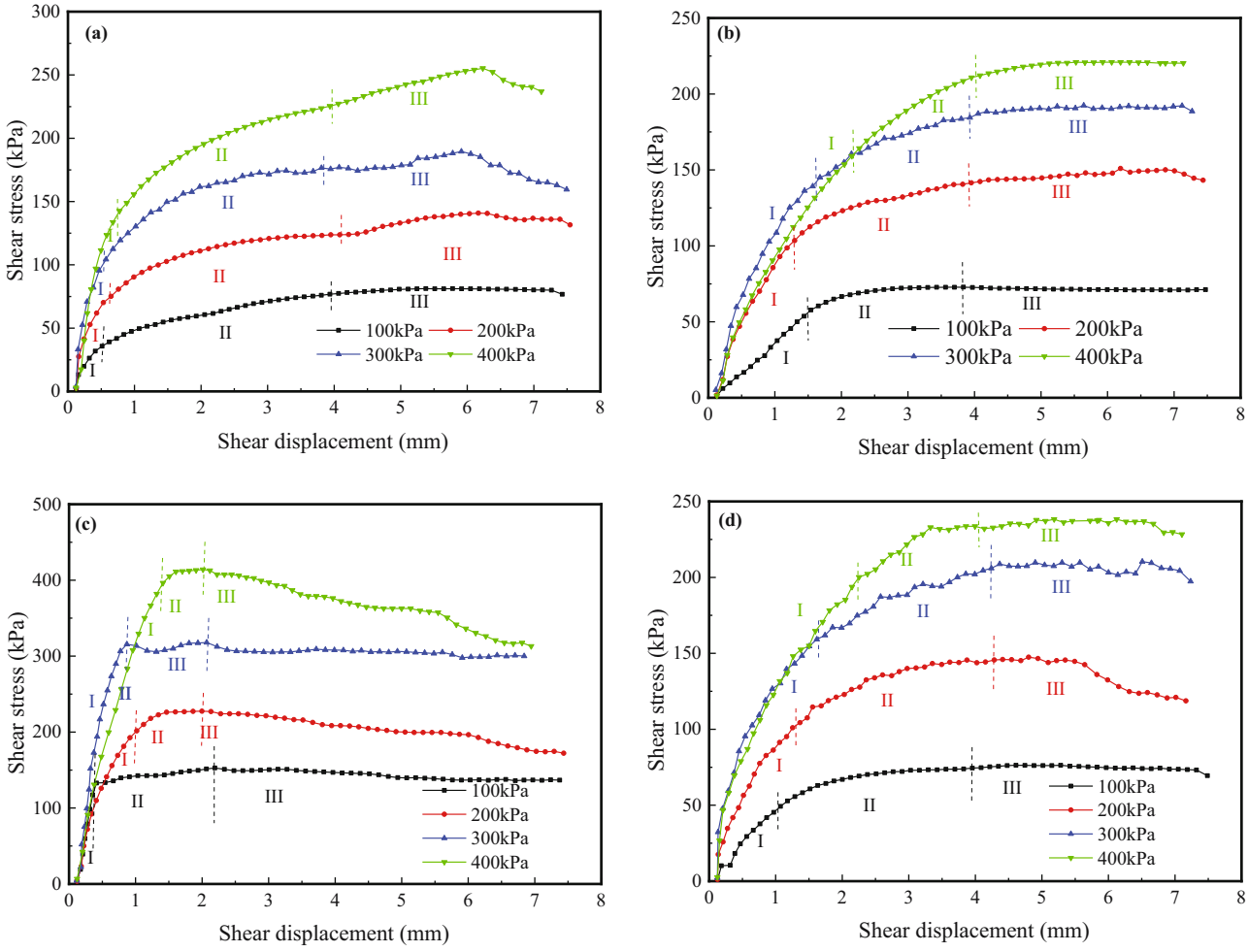

Figure 16: Shear stress–shear displacement curves of improved specimens of different materials: (a) straw; (b) starch; (c) cement; and (d) epoxy resin.

After the test piece mixed with cement was washed, a few cracks appeared on the upper surface, and part of the edge soil fell off. After the test piece mixed with epoxy resin was washed, a few shallow cracks appeared on the upper surface, and the test piece was relatively complete as a whole.

The scour coefficient of the raw soil material was obtained by the volume loss of scour. The larger the scour coefficient, the worse the scour resistance would be; otherwise, the better the scour resistance would be.

$$\alpha_{si} = \frac{V_0 - V_t}{V_0} \times 100\%, \quad (1)$$

where α_{si} denotes the scour coefficient; V_0 is the original volume; and V_t represents the volume corresponding to time t.

The loss coefficient was calculated according to formula (1), and the results are shown in Figure 18. According to the test phenomenon and Figure 18a, the scouring loss of pure yellow mud was the largest, up to 62.28%. With the increase in the straw content, the scouring coefficient first decreased and then increased. When the straw content was 0.5%, the scouring coefficient was the lowest, which was 46.4%. The main reason was that the surface of the straw was not smooth, which played a certain role in binding the soil. When the rain washed the test piece, the binding of the straw to the soil made the soil fall off more slowly, making the anti-scouring ability stronger. However, due to the hollow inner side of the straw, when the straw content was too much, there would be more pores in the soil, resulting in the decrease in the anti-scouring ability of the test piece. Accordingly, for the anti-scouring ability of the test piece, it was suggested that the content of straw should be controlled at 0.5%.

As depicted in Figure 18b, with the increase in the starch content, the scouring coefficient still decreased first and then increased. When the starch content was 5%, the scouring coefficient was the lowest, 47.38%. This was because the starch would expand when

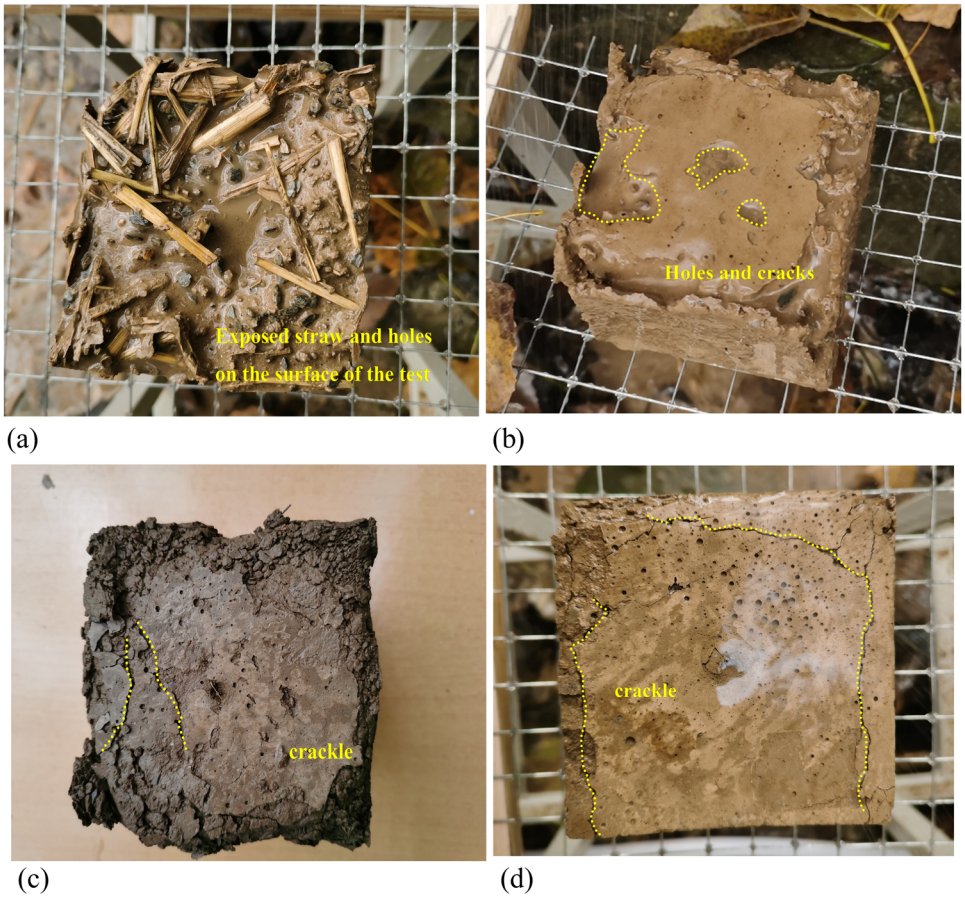

Figure 17: Test block after scouring: (a) straw; (b) starch; (c) cement; and (d) epoxy resin.

contacting water, and the particles would bond into a film and have a certain cementation, so the soil would be closely connected and could resist the scouring of rainwater to a certain extent. However, when the starch content was too high, the starch would be agglomerated, and the yellow mud was not wrapped with enough starch, so it would be easy to fall off in the face of rain erosion. Thus, it was suggested that the content of starch should be controlled at 5% for the anti-scouring ability of the specimen.

As depicted in Figure 18c, with the increase in the cement content, the scouring coefficient gradually decreases. Under different cement content, the anti-erosion loss rates of the specimens are 56.53, 40.9, 22.54, and 11.21% respectively, 9.23–82% lower than that of yellow mud specimens. A series of hydration reactions and hydrolysis reactions would occur in the process of cement as modified material. These reaction products would act together to form a raw soil skeleton and fill the pores of the soil. The reduction in pores would make the free water and air in the soil flow, which could improve the water resistance of the soil to a certain extent, so as to improve the anti-scouring ability of the specimen. According to the above analysis of the impact of straw and starch on the anti-scouring capacity of the specimen, the requirements were met when the scouring coefficient was 41%. According to the above analysis of the effect of cement on the shear strength of the specimen, combined with the anti-scouring coefficient of the specimen and the cement cost, it was suggested that the cement content should be controlled at 5% for the anti-scouring capacity of the specimen.

As depicted in Figure 18d, with the increase in epoxy resin content, the scouring coefficient gradually decreases. When the content was 7% or more, the scouring coefficient was stable at about 12%. The main reason was that the cross-linking reaction occurred after epoxy resin was mixed with the curing agent to form a 3D network structure to wrap the soil in it. In the face of the scouring of rainwater, the soil was difficult to fall off, thus enhancing the anti-scouring ability of the specimen. When the dosage was 7%, epoxy resin and yellow mud were fully combined and tended to be saturated. Accordingly, when the dosage increased again, it had a slight effect on the improvement

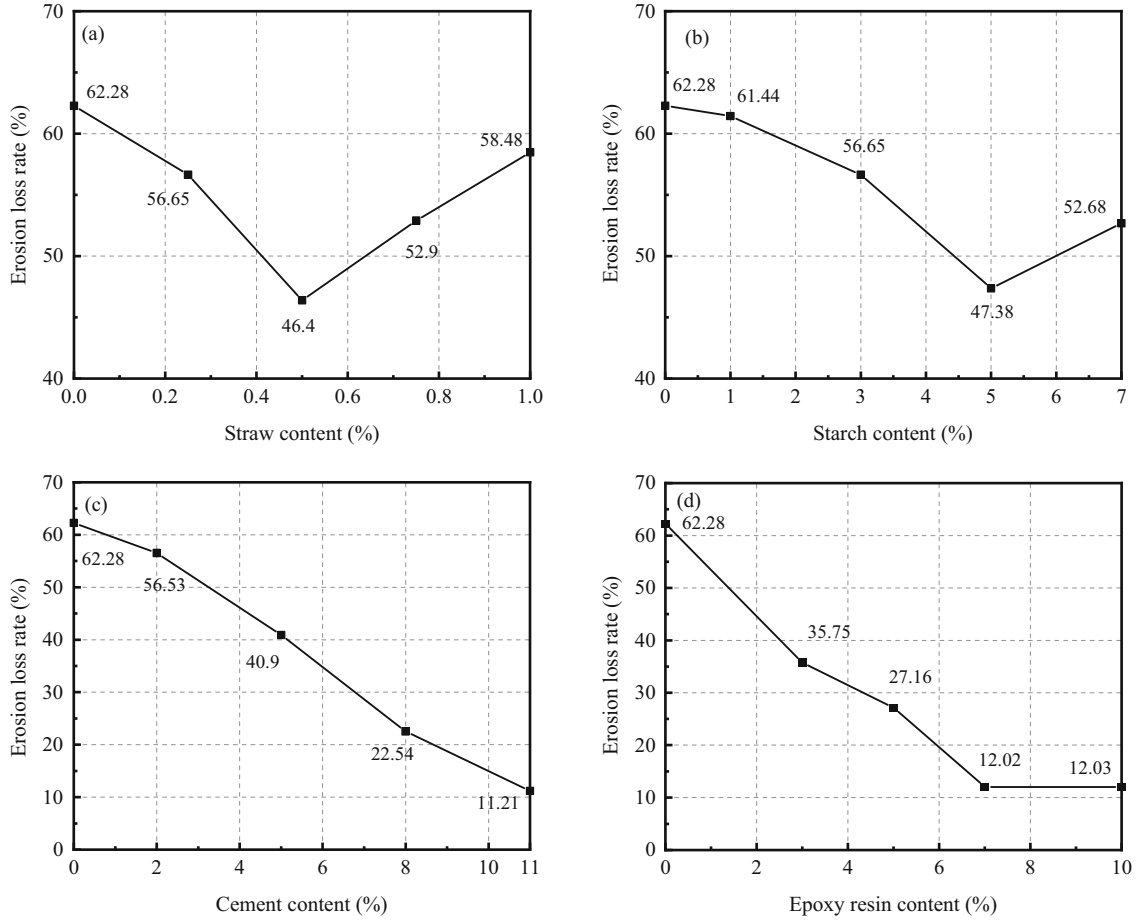

Figure 18: Erosion loss rate of different materials: (a) straw; (b) starch; (c) cement; and (d) epoxy resin.

of anti-scouring ability of yellow mud. Thus, it was suggested that the content of epoxy resin should be controlled at 7% for the anti-scouring capacity of the specimen.

3.3 Evaluation on the effect of improving yellow mud by different materials

To comprehensively evaluate the improvement effect of Qiang villages' yellow mud from two aspects of shear strength characteristics and scouring resistance, the shear strength ratio of the modified yellow mud and pure yellow mud was used to characterize the strength improvement effect, and the scouring coefficient was adopted to characterize the scouring resistance of the specimen. The larger the shear strength ratio, the smaller the scouring coefficient would be, and the better the improvement effect would be.

Figure 19 shows the comprehensive evaluation results of yellow mud improvement effect. The figure depicts that the comprehensive improvement effect of the test piece was better when the straw content was 0.5 and 0.75% (Figure 19a), and the shear strength and scouring resistance of yellow mud test piece were improved at the same time. As indicated by Figure 19b, when the starch content was 5 and 7%, the comprehensive improvement effect of the test piece was better. Figure 19c presents the evaluation of the improvement effect of the cement content on the yellow mud. As revealed by this figure, with the increase in the content, the comprehensive improvement effect was increased. According to the above analysis, combined with the cost of cement, in terms of improving the shear strength and scour resistance of yellow mud, the cement content is recommended to be controlled at 5%. As indicated by Figure 19d, when the content of epoxy resin was 7 and 10%, the comprehensive improvement effect of the test piece was better. Considering the environmental pollution, secondary utilization, and economic cost of each modified material, combined with the above improvement effect evaluation, it was suggested that the content of the modified materials included: straw content of 0.5%, starch content of 5%, cement content of 5%, and epoxy resin content of 7%.

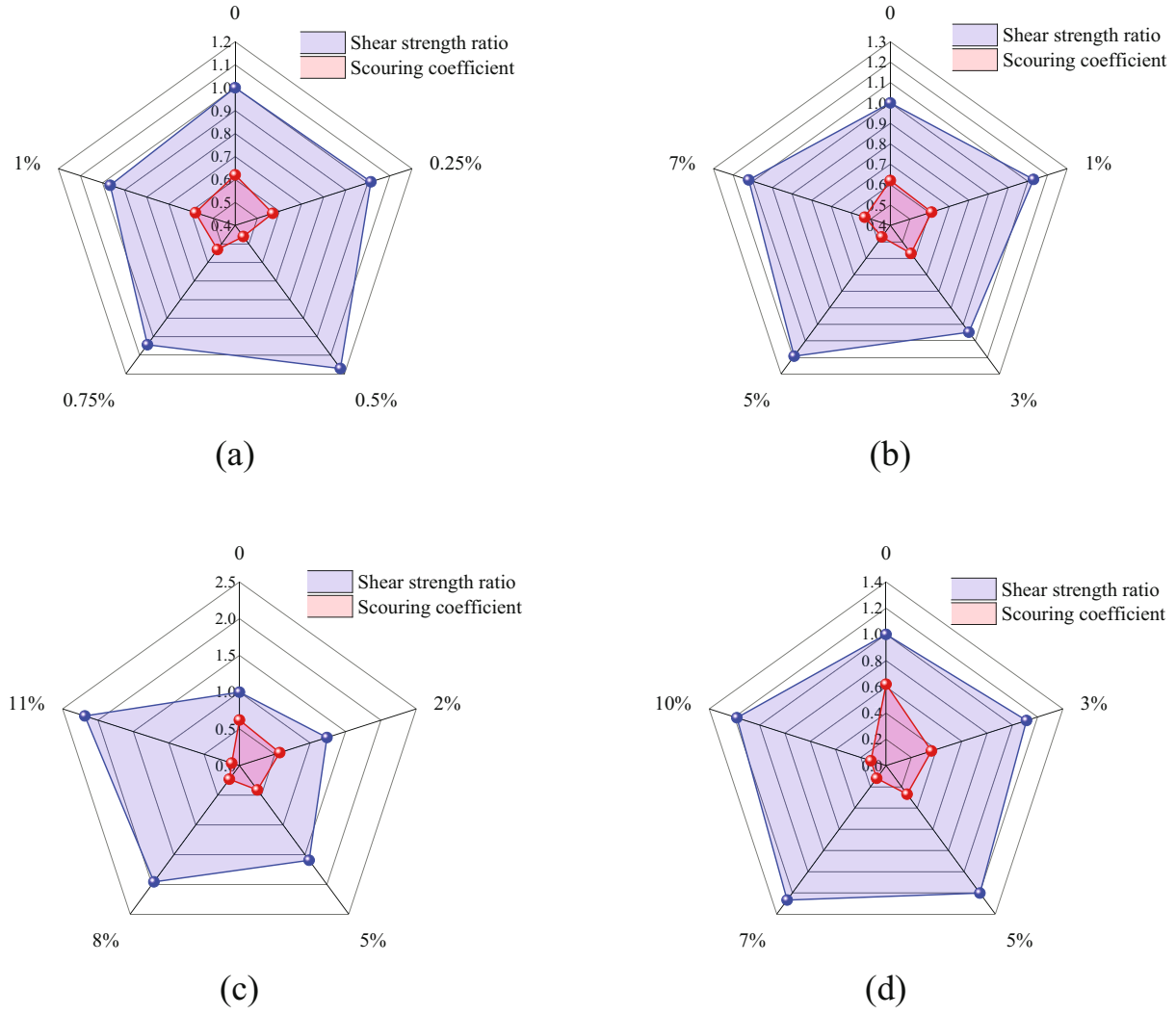

Figure 19: Effect of improving yellow mud with different materials: (a) straw; (b) starch; (c) cement; and (d) epoxy resin.

3.4 Influence mechanism of different material contents on loess strength

3.4.1 Qualitative description of SEM images

To explain the modification effect of yellow mud of Qiang Village mixed with straw, starch, cement, and epoxy resin from the micromorphology, the pure yellow mud and the samples mixed with different materials were analyzed by the SEM. The results are shown in Figure 20.

Figure 20(1) depicts the SEM figure of the yellow mud. As can be seen from the figure, the pores inside the pure yellow mud specimen were large and numerous, thus increasing the weak areas inside the specimen. Figure 20(1b) depicts that the soil mass of the specimen without materials was loose, and the soil particles were stacked together but not closely connected, which would be easy to be destroyed under the action of external forces. Accordingly, the strength of the pure yellow mud specimen was low, and the anti-erosion ability was poor.

Figure 20(2) depicts the SEM diagram of the sample mixed with straw. Straw acted as aggregate in the test piece and played a role of "reinforcement." The unsmooth surface of straw laid good mechanical bite conditions between the straw and yellow mud, as presented in Figure 20(2a). There were small grooves and spikes on the surface of straw, and soil particles were well attached to the surface of straw, which suggested that straw could increase the internal friction of raw soil test piece and pull the soil, so as to improve the shear strength and scouring resistance of the yellow mud. However, due to the hollow shape of straw (Figure 20(2b)), if the amount of straw was too high, these hollow areas would pass through the interior of the test piece, thus increasing the weak points of the test piece. In

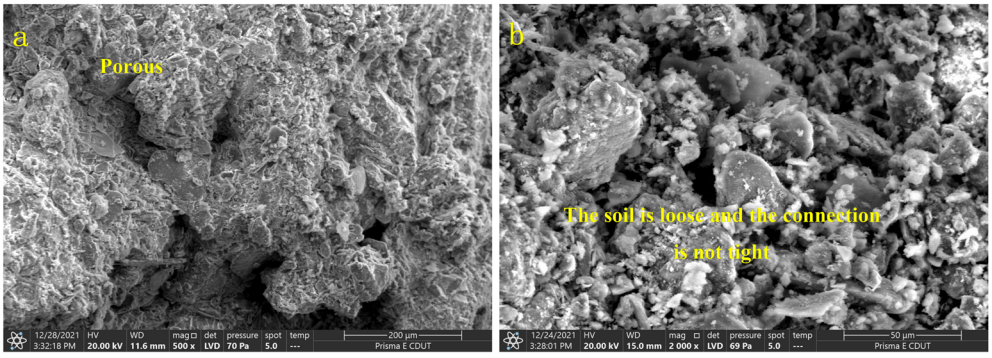

(1)

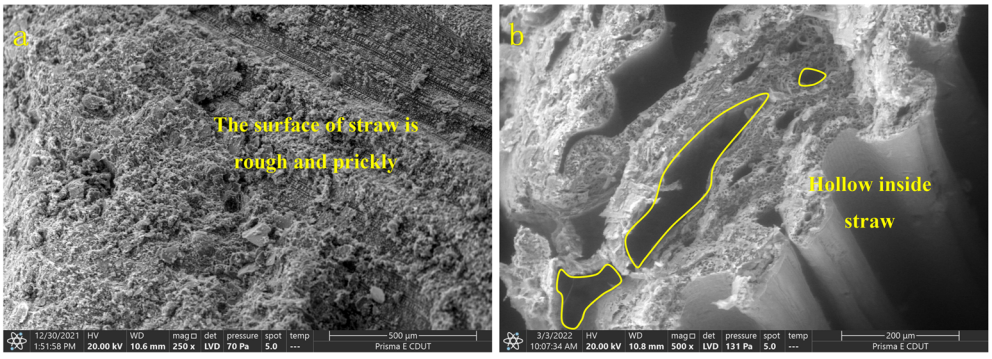

(2)

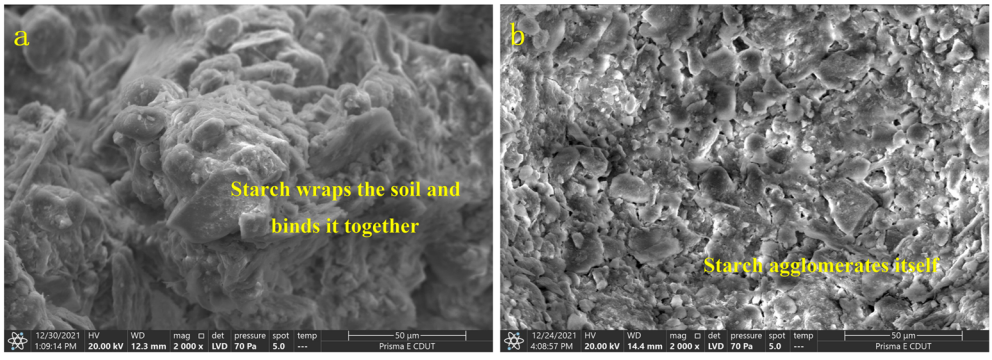

(3)

(4)

(*continue on the next page*)

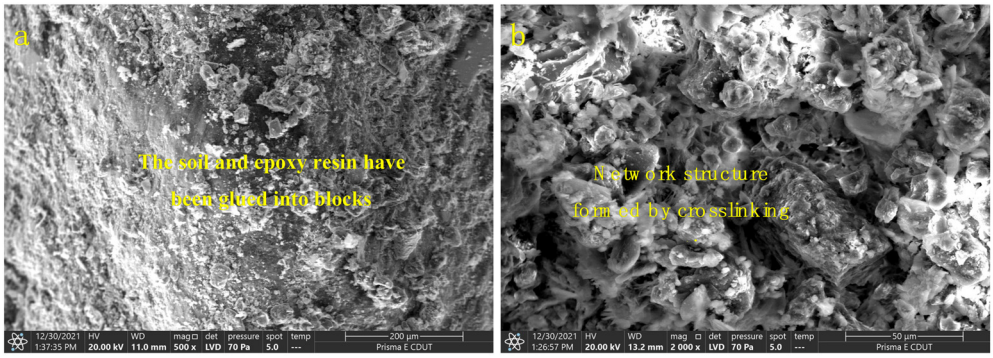

Figure 20: SEM images of specimens with different materials: (1) SEM of pure yellow mud; (2) SEM of straw-improved yellow mud; (3) SEM of starch-modified yellow mud; (4) SEM of cement-modified yellow mud; and (5) SEM of epoxy resin-modified yellow mud.

the modification process, the soil will not be closely combined, the moisture in the specimen will make the straw rotten and moldy in the curing process, resulting in a soft filling medium and weakened mechanical properties of the specimen, so the amount of straw should not be too high.

Figure 20(3) depicts the SEM diagram of starch-modified yellow mud. As indicated by Figure 20(3a), starch could be bonded into a film to wrap the soil and bond it together, which played a certain cementation role and made the soil bond more closely, so as to improve the strength and anti-scouring ability of the soil. However, when the starch content was too high, the starch would bond into a mass (Figure 20(3b)). The more these starch clusters inside the specimen, the easier it would be to destroy the specimen when receiving external force. Thus, the amount of starch should not be too high.

Figure 20(4) depicts the SEM figure of cement-modified yellow mud. As depicted in Figure 20(4b), hydration reaction and hydrolysis reaction would occur during cement modification of the yellow mud, and fibrous calcium silicate hydrate, CAH gel, calcium hydroxide, needle-like ettringite, and other substances would be generated. As depicted in Figure 20(4a), the pores of the specimens were significantly reduced, since these cementing substances and hydration products would adhere to the inner wall and surface of the pores between the soil particles, and also condense to form soil skeleton and reduce the pores between the soil particles. When the calcium, sodium, magnesium, and aluminum ions reacted with the ions adsorbed on the surface of soil particles, the ion exchange reaction could reduce the thickness of water film on soil particles, facilitate the coagulation of soil particles, enhance the strength of soil, and also improve the anti-scouring ability of soil to a certain extent.

Figure 20(5) depicts the SEM diagram of yellow mud modified by epoxy resin. As depicted in Figure 20(5a), the pores of specimens were significantly smaller than those of pure yellow mud. This was because epoxy resin was stable and had strong adhesion. Epoxy resin E-51 did not damage the soil. When it was mixed with curing agent, a cross-linking reaction occurred, as presented in Figure 20(5b). The 3D network structure generated by the cross-linking reaction connects the soil and forms a new skeleton to fill the void of the soil, thus improving the cohesion of the soil and enhancing its shear strength and anti-erosion ability. As indicated by Figure 20(5a), when epoxy resin content was 7%, the soil mass and epoxy resin were well combined and tended to be saturated. Accordingly, when the dosage was higher than 7%, the modification effect of epoxy resin on soil is no longer improved.

3.4.2 Quantitative analysis of PCAS operation

PCAS software was used to analyze the 500 times magnified SEM images of the specimens mixed with different materials. This software binarizes the images and obtains the binarized images and particle recognition results primarily based on the threshold segmentation method (Figure 21). After processing, the software automatically segmented and identified pores and particles, while eliminating impurities. After image processing, geometric parameters were automatically output, which consisted of porosity, area, perimeter, shape coefficient, probability entropy, and fractal dimension. The specimens with and without materials were quantitatively compared and analyzed to explain the structural characteristics of the specimens with different materials and the effects of shear

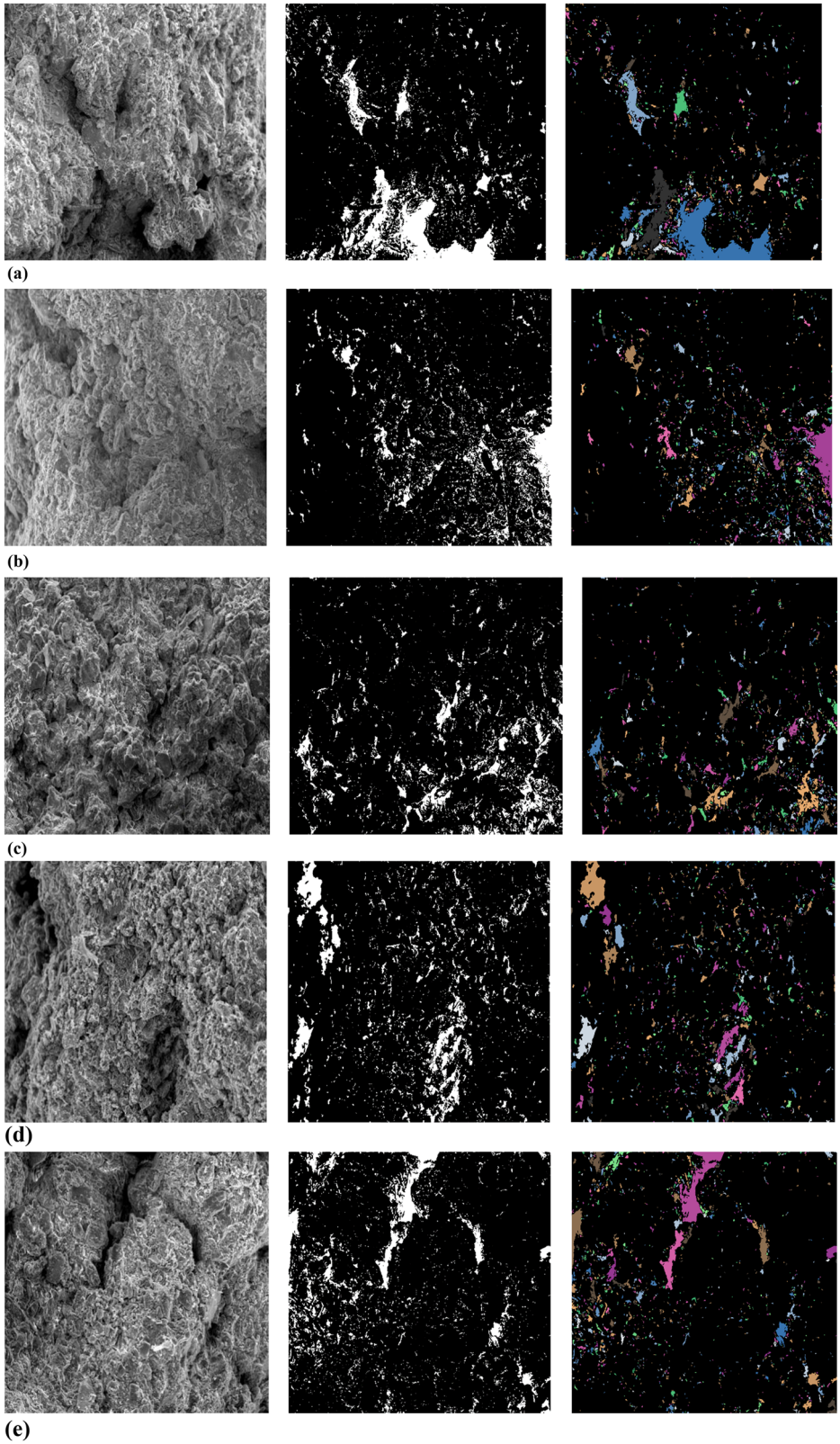

Figure 21: SEM images of specimens with different modified materials: (a) binarization graphics and particle recognition results of pure yellow mud specimens; (b) binary graphics and particle recognition results of specimens with straw; (c) binary graphics and particle recognition results of specimens with starch; (d) binary graphics and particle recognition results of specimens with cement; and (e) binary graphics and particle recognition results of specimens with epoxy resin.

Table 6: Pore classification

Classification	Microporosity	Small pores	Mesoporosity	Macroporosity
Pore radius (μm)	<2	2–5	5–20	>20

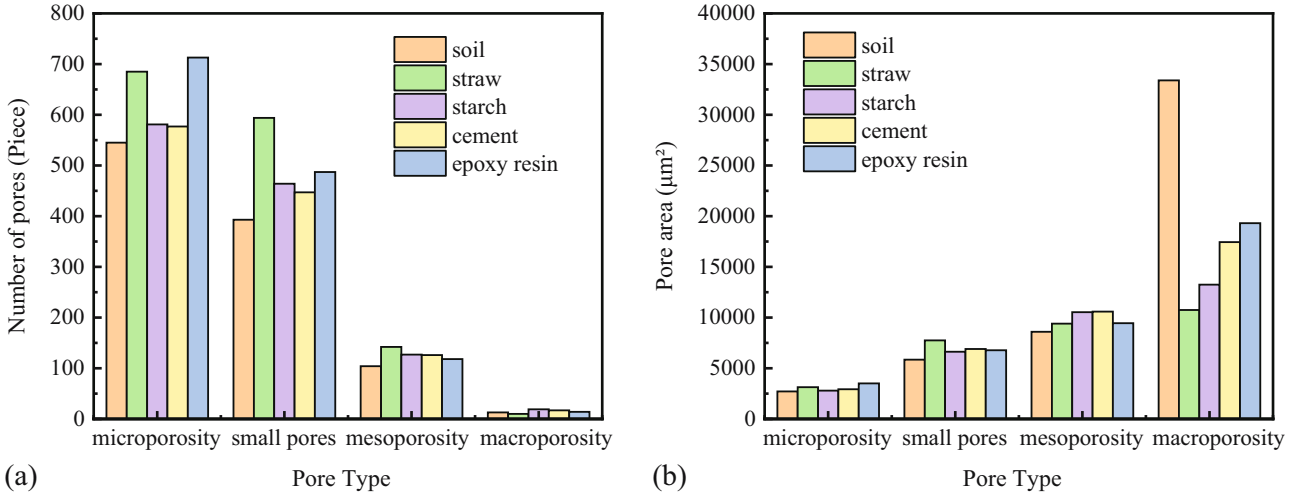

Figure 22: Pore area distribution of different materials: (a) pore number distribution and (b) pore area distribution.

strength and scouring resistance from a microscopic point of view. It is noteworthy that the length and area obtained by PCAS software were in pixels and should be converted into real parameters through equations (2) and (3).

$$S_t = S \times R^2, \tag{2}$$

$$C_t = C \times R, \tag{3}$$

where S_t and C_t represent the actual area and actual perimeter; S and C represent the pixel area and pixel perimeter; R is the resolution of the image (in this study, the sub-change in the 500 times magnified image is 0.54 μm per pixel)

In accordance with the classification criteria in Table 6, the number of pores and pore area of samples of different materials were statistically analyzed in the histogram. Figure 22 presents the statistical results. As depicted in Figure 22a, when the modified material was added to the yellow mud, the total number of macropores of the sample increased or changed insignificantly, and the micro pores increased.

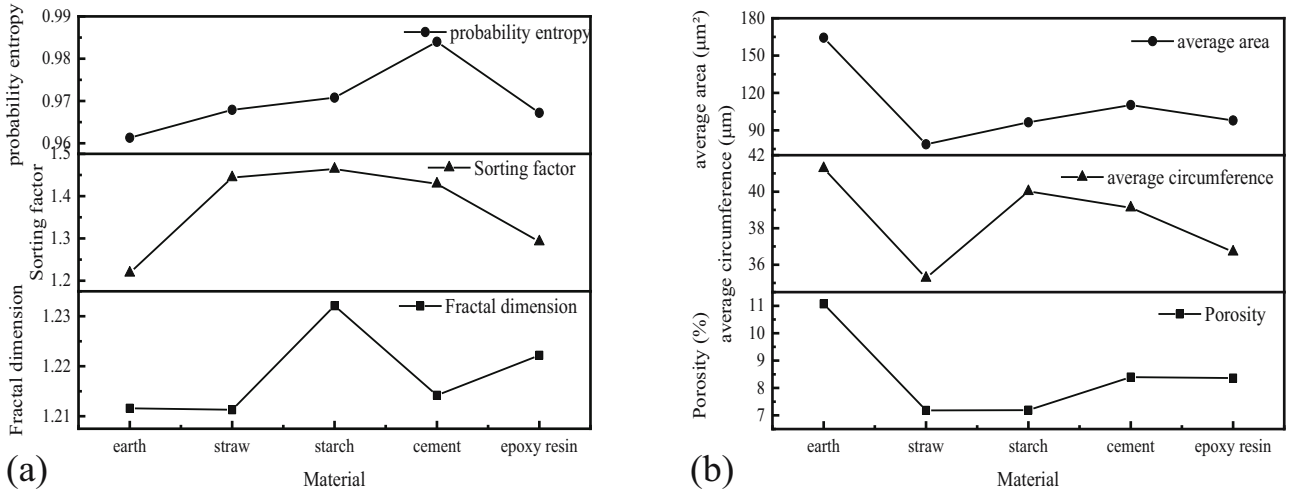

Figure 23: Parameter statistics: (a) fractal dimension, sorting factor, probability entropy; (b) porosity; average circumference; average area.

The modified yellow mud specimen primarily had micro pores. The total pore areas of the pure yellow mud specimen, the straw specimen, the starch specimen, the cement specimen, and epoxy resin specimen were 50553.5, 31034.6, 33209.2, 37866.3, and 39029.6 μm². As depicted in Figure 22b, the areas of micropores, small pores, and medium pores of the modified yellow mud test block were increasing, while the area of large pores was found as the largest of the pure yellow mud test piece. The pore area of the specimen was primarily dependent on the area of large and medium pores. Pure yellow mud specimens had large pore areas and low connection strength between the particles. When rainwater was immersed in the soil, or the soil was sheared by external force, the soil particles fell into the pores and would be more likely to be damaged. The pore area of the specimens with straw, starch, cement, and epoxy resin was relatively low and stable as compared with that of the yellow mud, so the shear strength and scouring resistance were found to be strong.

Probability entropy is capable of characterizing the orientation of particles and pores. When the value approached 1, the order of the specimen was worse, and the soil was more stable. The separation coefficient represents the uniformity of the particles. The larger the value, the worse the separation would be, the smaller the porosity and the more stable the soil would be. The average shape coefficient of particles represents the difference between the particle shape and sphere. The larger the fractal dimension, the more complex and stable the soil shape would be [39–41].

As depicted in Figure 23a, when the modified material was added to the yellow mud, the probability entropy of the specimen increased and approached 1 compared with the pure yellow mud, thus indicating that the pores of the modified specimen were randomly arranged. The order was poor, and the soil was more stable. Compared with pure yellow mud, the sorting coefficient of the samples with materials increased, which revealed that the modified yellow mud significantly changed the particle shape and poor sorting performance due to the binding effect of straw, the gelation of starch, the hydration and hydrolysate of cement, and the 3D network structure generated by the cross-linking reaction of epoxy resin. After starch, cement, and epoxy resin were added, the fractal dimension of the specimen increased, which revealed that soil particles in the specimen had a complicated morphology. There was little difference between the fractal dimension of straw and pure clay, since there was no significant difference between straw and pure clay.

The average pore area and average pore perimeter could reflect the pore size. The larger the value, the more the macropores would account for. Porosity is a vital parameter affecting water flow in pores. As depicted in Figure 23b, the average pore area of the test piece added with straw, starch, cement, and epoxy resin decreased by 52.08, 41.36, 32.92, and 40.42% compared with those of the yellow mud test piece, the average perimeter was reduced by 14.56, 3.05, 5.23, and 11.07% as compared with that of the yellow mud test piece, and the porosity decreased by 35.14, 35.05, 24.12, and 24.28% compared with that of the yellow mud test piece. The three indexes of the pure yellow mud specimen were found to be large, which suggested that the pore size was large, the proportion of macropores was large, the soil structure was loose, and it would be easy to be damaged under the action of external force. In contrast, the specimen with material exhibited low porosity, inhibited the flow of water in the pores, and improved its shear strength and scouring resistance.

4 Conclusion

Based on the shear resistance and scour resistance of yellow mud of Qiang Village, the direct shear test, scour resistance test, and microstructure analysis of straw, starch, cement, and epoxy resin as modified materials were performed in this study. The main conclusions are drawn as follows:

(1) Straw, starch, and epoxy resin all improved their shear strength and anti-scour ability, and all showed peaks in their performance-content curves. The optimal dosage of straw was 0.5%, that of starch was 5%, and that of epoxy resin reached 7%.
(2) Cement was found with a unidirectional change in its performance-content curve, thus having a significant improvement effect. In accordance with the improvement of shear strength and anti-scour ability with the cost of cement, this study suggested that the cement content should be controlled to be 5%.
(3) According to the micromorphology analysis of the respective specimen, the modification effect of straw on yellow mud was mainly dependent on its binding effect on soil, that of starch on yellow mud was primarily dependent on its own gelation, that of cement on yellow mud largely depended on its hydration reaction and hydrolysis reaction, and that of yellow mud by epoxy resin mainly relied on the 3D network structure formed by its crosslinking reaction.
(4) According to the data output from the SEM image of the specimen processed by PCAS software, after the addition of the modified material, the total pore area of the specimen was less than that of the pure yellow

mud specimen, and the pores were mainly micro pores. The micro pore area of the modified yellow mud increased, while the macro pore area decreased.

In this study, the properties of straw, starch, cement, and epoxy resin to improve the yellow mud in Qiang Village were investigated, and a novel idea was proposed for earthquake disaster reduction in Qiang Village. However, the test results revealed that the respective material could have different modification effects on different properties of yellow mud. Subsequent studies can attempt to compound the above materials to supplement each other's deficiencies and achieve better results.

Acknowledgments: We thank our research classmates for their valuable work and providing experiment data and anonymous reviewer for his critiques and comments.

Funding information: This study was supported by State Key Laboratory of Geohazard Prevention and Geoenvironment Protection (No. SKLGP2020K010). Project is supported by Chinese Government Scholarship (CSC No. 201906560013).

Author contributions: All authors have accepted responsibility for the entire content of this manuscript and approved its submission.

Conflict of interest: The authors state no conflict of interest.

References

[1] Wang, J. W., X. L. Chen, L. Y. Zhang, M. D. Jin, and D. G. Yu. Empowerment for community-based tourism in ethnic minority village: A case study of Shiyi Qiang Stockaded village, China. *Journal of Zhejiang University*, Vol. 48, No. 1, 2021, pp. 107–117, 130.

[2] Liu, X. J., X. Zheng, W. C. Cheng, Q. Kong, and J. J. Wang. The shear strength of the nature loess joint: A case study in Shaanxi province. *Journal of Testing and Evaluation*, Vol. 47, No. 3, 2019, pp. 2297–2312.

[3] Luo, Y., B. T. Yin, X. Q. Peng, Y. Y. Xu, and L. Zhang. Wind-rain erosion of Fujian Tulou Hakka Earth Buildings. *Sustainable Cities and Society*, Vol. 50, 2019, id. 101666.

[4] Traore, L. B., C. Ouellet-Plamondon, A. Fabbri, F. McGregor, and F. Rojat. Experimental assessment of freezing-thawing resistance of rammed earth buildings. *Construction and Building Materials*, Vol. 274, 2021, id. 121917.

[5] Walker, P., B. V. V. Reddy, and M. Mani. Preface for SI: Modern earth building materials and technologies preface. *Construction and Building Materials*, Vol. 262, 2020, id. 120663.

[6] He W., L. Y. Wang, W. J. Yu, G. J. Zhang, B. Zhong, S. Liao, et al. Prevalence and spatial distribution patterns of human echinococcosis at the township level in Sichuan Province, China. *Infectious Diseases of Poverty*, Vol. 10, No. 1, 2021, id. 82.

[7] Schwerdt, S., D. Mirschel, T. Hildebrandt, M. Wilke, and P. Schneider. Substitute building materials in geogrid-reinforced soil structures. *Sustainability*, Vol. 13, No. 22, 2021, id. 12519.

[8] Adhikari, T., R. Dharmarajan, D. Lamb, and H. M. Zhang. Remediation of Frogmore mine spoiled soil with nano enhanced materials. *Soil & Sediment Contamination*, Vol. 31, No. 3, 2022, pp. 367–385.

[9] Xu, Z., Z. P. Huang, C. J. Liu, X. W. Deng, D. Hui, S. J. Deng, et al. Research progress on mechanical properties of geopolymer recycled aggregate concrete. *Reviews on Advanced Materials Science*, Vol. 60, No. 1, 2021, pp. 158–72.

[10] Xu, Z., Z. P. Huang, C. J. Liu, H. Deng, X. W. Deng, D. Hui, et al. Research progress on key problems of nanomaterials-modified geopolymer concrete. *Nanotechnology Reviews*, Vol. 10, No. 1, 2021, pp. 779–92.

[11] Liang, M. A., L. Lu, H. J. He, J. X. Li, Z. Q. Zhu, and Y. N. Zhu. Applications of biochar and modified biochar in heavy metal contaminated soil: A descriptive review. *Sustainability*, Vol. 13, No. 24, 2020, id. 14041.

[12] Zhang, K., B. R. Lu, Y. H. Wang, Z. J. Lei, and Z. S. Yang. Experimental strength of earth-based construction materials in different regions of China. *Advances in Materials Science and Engineering*, Vol. 2019, 2019, id. 8130743.

[13] Damme, H. V. and H. Houben. Earth concrete. stabilization revisited. *Cement and Concrete Research*, Vol. 114, 2017, pp. 90–102.

[14] Miccoli, L., U. Muller, and S. Pospisill. Rammed earth walls strengthened with polyester fabric strips: Experimental analysis under in-plane cyclic loading. *Construction and Building Materials*, Vol. 149, 2017, pp. 29–36.

[15] Zhao, Y. Y., X. Z. Ling, W. G. Gong, P. Li, G. Y. Li, and L. N. Wang. Mechanical properties of fiber-reinforced soil under triaxial compression and parameter determination based on the Duncan-Chang model. *Applied Science* (*Basel*), Vol. 10, No. 24, 2020, id. 9043.

[16] Xu, Z., Z. P. Huang, C. J. Liu, X. W. Deng, D. Hui, Y. T. Deng, et al. Experimental study on mechanical properties and microstructures of steel fiber-reinforced fly ash metakaolin geopolymer-recycled concrete. *Reviews on Advanced Materials Science*, Vol. 60, No. 1, 2021, pp. 578–90.

[17] Xu, Z., J. N. Wu, M. Zhao, Z. J. Bai, K. Y. Wang, J. W. Miao, et al. Mechanical and microscopic properties of fiber-reinforced coal gangue-based geopolymer concrete. *Nanotechnology Reviews*, Vol. 11, No. 1, 2022, pp. 526–543.

[18] Liu, C., Y. R. Lv, X. J. Yu, and X. Wu. Effects of freeze-thaw cycles on the unconfined compressive strength of straw fiber-reinforced soil. *Geotextiles and Geomembranes*, Vol. 48, No. 4, 2020, pp. 581–590.

[19] Li, L. H., T. B. Zang, H. L. Xiao, W. Q. Feng, and Y. L. Liu. Experimental study of polypropylene fibre-reinforced clay soil mixed with municipal solid waste incineration bottom ash. *European Journal of Environmental and Civil Engineering*, Vol. 2020, 2020, id. 1795726.

[20] Sujatha, E. R., P. Atchaya, S. Darshan, and S. Subhashini. Mechanical properties of glass fibre reinforced soil and its application as subgrade reinforcement. *Road Materials and Pavement Design*, Vol. 22, No. 10, 2021, pp. 2384–2395.

[21] Tang, H., H. H. Li, Z. Duan, C. Y. Liu, G. N. Wu, and J. Z. Luo. Direct shear creep characteristics and microstructure of fiberreinforced soil. *Advanced Civil Engineering*, Vol. 2021, 2021, id. 8836293.
[22] Zhang, K., B. R. Lu, Y. H. Wang, Z. Qu, and L. Qu. Study on the modification formula of earth material compound with cement and gravel by single lattice theory. *Advanced Civil Engineering*, Vol. 2020, 2020, id. 8136570.
[23] Arslan, M. E., M. Emiroğlu, and A. Yalama. Structural behavior of rammed earth walls under lateral cyclic loading: A comparative experimental study. *Construction and Building Materials*, Vol. 133, 2017, pp. 433–442.
[24] Han, C. P., Q. J. Dong, and X. B. Xu. Microstructural analysis on the variation of resilient modulus of lime modified soil under freezing-thawing action. *Road Materials and Pavement Design*, Vol. 2021, 2021, id. 1924235.
[25] Khadka, S. D., P. W. Jayawickrama, S. Senadheera, and B. Segvic. Stabilization of highly expansive soils containing sulfate using metakaolin and fly ash based geopolymer modified with lime and gypsum. *Transportation Geotechnics*, Vol. 23, 2020, id. 100327.
[26] Seco, A., J. M. del Castillo, S. Espuelas, S. Marcelino-Sadaba, and B. Garcia. Stabilization of a clay soil using cementing material from spent refractories and ground-granulated blast furnace slag. *Sustainability*, Vol. 13, No. 6, 2021, id. 3015.
[27] Miranda, T., R. A. Silva, D. V. Oliveira, D. Leitao, N. Cristelo, J. Oliveira, et al. ICEBs stabilised with alkali-activated fly ash as a renewed approach for green building: Exploitation of the masonry mechanical performance. *Construction and Building Materials*, Vol. 155, 2017, pp. 65–78.
[28] Xu, J. B., Y. Z. Luo, Y. Z. Wang, C. G. Yan, L. J. Zhang, L. H. Yin, et al. Triaxial axis shear mechanical properties of fiber-reinforced foamed lightweight soil. *Journal of Materials in Civil Engineering*, Vol. 33, No. 4, 2021, id. 04021047.
[29] Yue, H. F., A. G. Fang, S. D. Hua, Z. H. Gu, Y. Jia, and C. Yang. Development and field application of phosphogypsum-based soil subgrade stabilizers. *Journal of Renewable Materials*, Vol. 10, No. 8, 2022, pp. 2247–2261.
[30] Portelinha, F. H. M., N. D. Correia, I. D. Mendes, and J. W. B. Da Silva. Geotechnical properties and microstructure of a diesel contaminated lateritic soil treated with lime. *Soil & Sediment Contamination*, Vol. 30, No. 7, 2021, pp. 838–861.
[31] Nath, S. K., N. S. Randhawa, and S. Kumar. A review on characteristics of silico-manganese slag and its utilization into construction materials. *Resources, Conservation and Recycling*, Vol. 176, 2022, id. 105946.
[32] Lai, W. Y., S. J. Li, Y. A. Li, and X. H. Tian. Air pollution and cognitive functions: Evidence from straw burning in China. *American Journal of Agricultural Economics*, Vol. 104, No. 1, 2022, pp. 190–208.
[33] Costa, S., D. Summa, F. Zappaterra, R. Blo, and E. Tamburini. Aspergillus oryzae grown on rice hulls used as an additive for pretreatment of starch-containing wastewater from the pulp and paper industry. *Fermentation*, Vol. 7, No. 4, 2021, id. 317.
[34] Krzywinski, K., L. Sadowski, and M. Piechowka-Mielnik. Engineering of composite materials made of epoxy resins modified with recycled fine aggregate. *Science and Engineering of Composite Materials*, Vol. 28, No. 1, 2021, pp. 276–284.
[35] Di Remigio, G., I. Rocchi, and V. Zania. New method for a SEM-based quantitative microstructural clay analysis-MiCA. *Applied Clay Science*, Vol. 214, 2021, id. 106248.
[36] Ni, H. Y., J. F. Liu, B. X. Huang, H. Pu, Q. B. Meng, Y. G. Wang, et al. Quantitative analysis of pore structure and permeability characteristics of sandstone using SEM and CT images. *Journal of Natural Gas Science and Engineering*, Vol. 88, 2021, id. 103861.
[37] Bizhani, M., O. H. Ardakani, L. J. Knapp, and T. Akai. Quantitative analysis of statistical properties of organic-rich mudstone using large field-of-view SEM images. *Journal of Natural Gas Science and Engineering*, Vol. 95, 2021, id. 104238.
[38] Chen, L. J., X. J. Chen, X. Yang, P. Y. Bi, X. Ding, X. Huang, et al. Effect of calcium carbonate on the mechanical properties and microstructure of red clay. *Advances in Materials Science and Engineering*, Vol. 2020, 2020, id. 5298186.
[39] Zhang, B., J. Xin, L. Liu, L. J. Guo, and K. I. Song. An experimental study on the microstructures of cemented paste backfill during its developing process. *Advances in Civil Engineering*, Vol. 2018, 2018, id. 9783046.
[40] Miao, F. S., Y. P. Wu, Y. H. Xie, L. W. Li, J. Li, and L. Huang. Influence of permeation effect on themicrofabric of the slip zone soils: A case study from the Huangtupo landslide. *Journal of Mountain Science*, Vol. 16, No. 6, 2019, pp. 1231–1243.
[41] Qin, X. B., P. Wang, L. Liu, M. Wang, and J. Xin. Sensitivity analysis of microstructure parameters and mechanical strength during consolidation of cemented paste backfill. *Mathematical Problems in Engineering*, Vol. 2018, 2018, id. 5170721.